



## Dynamics of the Askja caldera July 2014 landslide, Iceland, from seismic signal analysis: precursor, motion and aftermath

Anne Schöpa<sup>1</sup>, Wei-An Chao<sup>2</sup>, Bradley Lipovsky<sup>3</sup>, Niels Hovius<sup>1,4</sup>, Robert S. White<sup>5</sup>, Robert G. Green<sup>5,1</sup>, Jens M. Turowski<sup>1</sup>

<sup>1</sup>Helmholtz Centre Potsdam GFZ German Research Centre for Geosciences, 14473 Potsdam, Germany

<sup>2</sup>Department of Civil Engineering, National Chiao Tung University, Hsinchu 300, Taiwan

<sup>3</sup>Department of Earth and Planetary Sciences, Harvard University, Cambridge, MA 02138, USA

<sup>4</sup>Institute of Earth and Environmental Science, University of Potsdam, 14476 Potsdam, Germany

<sup>5</sup>Department of Earth Sciences, University of Cambridge, Cambridge CB3 0EZ, UK

10 *Correspondence to:* Anne Schöpa ([schoepa@gfz-potsdam.de](mailto:schoepa@gfz-potsdam.de))

**Abstract.** Using data from a network of 58 seismic stations, we characterise a large landslide that occurred at the southeastern corner of the Askja caldera, Iceland, on 21 July 2014, including its precursory tremor and mass wasting aftermath. Our study is motivated by the need for deeper generic understanding of the processes operating not only at the time of catastrophic slope failure, but also in the preparatory phase and during the transient into the subsequent stable state.

15 In addition, it is prompted by the high hazard potential of the steep caldera lake walls at Askja as tsunami waves created by the landslide reached famous tourist spots 60 m above the lake level. Since direct observations of the event are lacking, the seismic data give valuable details on the dynamics of this landslide episode. The excellent seismic data quality and coverage of the stations of the Askja network made it possible to jointly analyse the long- and short-period signals of the landslide to obtain information about the triggering, initiation, timing, and propagation of the slide. The seismic signal analysis and a  
20 landslide force history inversion of the long-period seismic signals showed that the Askja landslide was a single, large event starting at the SE corner of the caldera lake at 23:24:05 UTC and propagating to the NW in the following 2 min. The bulk sliding mass was  $7\text{--}16\times 10^{10}$  kg, equivalent to a collapsed volume of  $35\text{--}80\times 10^6$  m<sup>3</sup>, and the centre of mass was displaced horizontally downslope by  $1260\pm 250$  m during landsliding. The seismic records of stations up to 30 km away from the landslide source area show a tremor signal that started 30 min before the main landslide failure. It is harmonic, with a  
25 fundamental frequency of 2.5 Hz and shows time-dependent changes of its frequency content. We attribute the complex tremor signal to accelerating and decelerating stick-slip motion on failure planes at the base and the sides of the landslide body. The accelerating motion culminated in aseismic slip of the landslide visible as a drop in the seismic amplitudes down to the background noise level 2 min before the landslide high-energy signal begins. We propose that the seismic signal of the precursory tremor may be developed as an indicator for landslide early-warning systems. The 8 hours after the main  
30 landslide failure are characterised by smaller slope failures originating from the destabilised caldera wall decaying in frequency and magnitude. We introduce the term afterslides for this subsequent, declining slope activity after a large landslide.



## 1 Introduction

Volcanic edifices are prone to landsliding because of their usually steep topography, fresh, unconsolidated deposits, and high seismic, volcanic and hydrothermal activity, and the associated surface deformation. Tsunami-creating landslides at volcanic edifices have often led to the destruction of infrastructure and high numbers of fatalities. For example, the 1792 Unzen  
5 Mayu-Yama, Japan, landslide and the resulting tsunami killed more than 15,000 people in the Shimabara Bay (Sassa et al., 2016) and the eruption of Mt. St. Helens on 18 May 1980 initiated a  $2.3 \times 10^9 \text{ m}^3$  landslide that ran into Spirit Lake and caused a 260-m-high wave deforesting adjoining slopes (Voight et al., 1981). Seismic networks are often installed around volcanoes for monitoring of magmatic processes and eruption forecasting. Their seismic records can also hold valuable information about landslide events occurring on the edifice.

10 Seismic signals of landslides are a powerful tool to reconstruct the dynamics of the slope failure including source mechanisms, the failure sequence together with precursory activity, and landslide properties (Brodsky et al., 2003; Favreau et al., 2010; Schneider et al., 2010; Moretti et al., 2012; Allstadt, 2013; Yamada et al., 2013). Long-period seismic signals of landslides from stations several thousand kilometres away can be used as references for inversions (Allstadt, 2013; Ekström and Stark, 2013; Yamada et al., 2013; Hibert et al., 2015; Chao et al., 2016) or models (Brodsky et al., 2003; Favreau et al.,  
15 2010; Schneider et al., 2010; Moretti et al., 2012) to constrain the location, mass, duration, displacement, and run-out trajectories of the landslide. Short-period waves, generated by the momentum exchanges within a granular landslide mass and along its boundaries, have been used to study the detachment, moving and reposing phases of landslides (Norris, 1994; Suriñach et al., 2005; Dammeier et al., 2011; Hibert et al., 2011, 2014; Deparis et al., 2008; Vilajosana et al., 2008). Seismic records can also give valuable information about triggers and precursors of slope failures (Amitrano et al., 2005; Caplan-  
20 Auerbach and Huggel, 2007; Senfaute et al., 2009; Got et al., 2010; Helmstetter and Garambois, 2010; Dietze et al., 2017). Repeated small earthquakes indicative of stick-slip movement on a small patch were observed before a landslide failed within shale and tuff layers in Rausu, Japan (Yamada et al., 2016). Individual cracking events that occur more frequently in time closer to the main failure were identified at a station 200 m away from the steep, bedrock source area of a  $10^4 \text{ m}^3$  landslide in the Illgraben, Switzerland (Zeckra et al., 2015). Continuous tremor was also described before ice-rock  
25 avalanches (Caplan-Auerbach et al., 2004; Huggel et al., 2008), during ice-sheet and glacial sliding (Lipovsky and Dunham, 2016), and iceberg collisions (MacAyeal et al., 2008; Martin et al., 2010). However, the localisation and characterisation of seismic tremor before mass wasting events is often limited by a sparse seismic station coverage, preventing a detailed analysis of the underlying source mechanisms.

In this study, we present seismic data from the 2014 Askja landslide. As the landslide was located in the centre of a  
30 temporary local network of 58 seismic stations the spatial coverage is exceptionally good and the signal-to-noise ratio of most stations is very high due to their remote locations far away from roads or other places of human activity. The excellent seismic data quality allows for a detailed reconstruction of the landslide dynamics based on the combined analysis of records from stations within a few kilometres of the landslide and at distances of up to 100 km. A force history inversion of the long-



period signals of the landslide from distant seismic stations of the network is used to infer its timing, propagation direction, mass and vertical and horizontal displacement. The short-period signals of nearby stations are included in a comprehensive interpretation of the landslide dynamics. These signals also contain information about the processes occurring before and after catastrophic slope failure. We identified a tremor signal in the seismic data of 38 stations located up to 30 km away  
5 from the landslide source area. We attribute the tremor and its time-dependent frequency changes to evolving stick-slip motion along sliding patches at the base of the landslide in the run up to catastrophic failure. After the catastrophic failure of the landslide, the seismic stations a few kilometres from the landslide source area recorded smaller slope failures. These smaller rockfalls and slides initiated from the destabilised section of the caldera wall where the large landslide originated from.

## 10 **2 The Askja landslide and its failure preconditions**

In the following, we first report on the Askja landslide and introduce the reader to the Askja area before we describe the factors that made the landslide source area prone to slope failure. We then focus on the seismic dataset and use it to characterise the landslide and the precursory tremor.

In the late evening of 21 July 2014, a steam cloud was seen rising over the Askja central volcano in the Icelandic highlands  
15 (Helgason et al., 2014). Field investigations on the following days revealed that a voluminous landslide must have occurred during the night, originating from the southeastern shore of the Askja caldera lake Öskjuvatn, where steep scars and fresh, mobilised material could be seen (Vogfjörd et al., 2015). Parts of the landslide material must have entered the lake and created tsunami waves as flood marks up to 60-80 m above the lake level were found at the shorelines (Gylfadóttir et al., 2015). The flood marks implied that up to ten individual waves inundated the shore and also went into the 200 m wide Víti  
20 crater, a popular tourist spot on the northeastern side of the lake. Analysis of the seismic record of the permanent stations of the Icelandic Meteorological Institute showed that the landslide occurred at 23:24 UTC, equivalent to local time (Saemundsson et al., 2015). This timing meant that no eyewitnesses were present. Geodetic surveys estimated the landslide volume to be  $12\text{--}50 \times 10^6 \text{ m}^3$  and that about  $10 \times 10^6 \text{ m}^3$  entered the caldera lake creating the tsunami waves (Gylfadóttir et al., 2017).

25 Several factors made the site at the southeastern corner of Lake Öskjuvatn prone to slope failures. These factors are: (i) the geological structures of a young collapse caldera with steeply dipping caldera ring faults; (ii) the geothermal system in this corner of the lake with hydrothermally altered volcanic rocks at the surface and earthquakes at 2-4 km b.s.l.; and (iii) the weather conditions in summer 2014 with sustained high temperatures and high precipitation amounts during the days before the landslide. We describe these failure preconditions below.



## 2.1 Geological setting

The Askja volcanic system is located in the Northern Volcanic Zone of Iceland and consists of a prominent central volcano and an associated fissure swarm. The shape of the Askja central volcano is dominated by nested calderas. The 7–9 km wide outer caldera (Askja caldera) developed in the early Holocene, and the 3–5 km wide inner caldera (Öskjuvatn caldera) with the lake Öskjuvatn gradually subsided in the 40 years following a rifting event in 1874–1876 (Acocella et al., 2015). The ring faults of the inner caldera dissect Pleistocene glaciovolcanic deposits of the Austurfjöll and the Thorvaldsfjall mountains at the eastern and southern margin of Lake Öskjuvatn (Fig. 1). There, the steep relief of up to 350 m is dominated by nearly vertically dipping fault surfaces of the cliffs and talus cones (Sigvaldason, 2002). The caldera ring faults were the location of minor effusive eruptions in the 20<sup>th</sup> century, that formed, among others, the lavas Suðurbotnahraun, where the landslide originated, and Kvíslahraun in the southeastern corner of the lake in 1922/23 (Hartley and Thordarson, 2012). The last eruptive activity at Askja occurred in 1961 when the Vikrahraun lava flowed out of a fissure at the northern rim of the Holocene Askja caldera (Thorarinsson and Sigvaldason, 1962). During the last decades, continuous subsidence has dominated the Askja caldera (Einarsson, 1991; de Zeeuw-van Dalssen et al., 2013), associated with contraction of an inferred shallow magma body, and the large-scale rifting of Iceland at a rate of 18.2 mm yr<sup>-1</sup> and an azimuth direction of 106° (DeMets et al., 1994). Nevertheless, fumarolic activity persists at the northern lakeshore in the vicinity of the Viti crater, and at the eastern and southern corner of the lake.

## 2.2 Seismicity

In the region of the Askja volcanic system, earthquakes occur at two levels in the crust, as shallow crustal seismicity between the surface and mostly 5 km depth, and as deep seismicity in the ductile lower crust at depths of 10–35 km, with magnitudes of usually  $M_L < 3$  (Jakobsdóttir et al., 2002; Soosalu et al., 2010; Greenfield et al., 2015).

The deep crustal earthquakes are located in distinct regions, beneath Kollóttadyngja shield volcano to the north, beneath the hyaloclastite mountain Upptyppingar to the east, location of a dyke intrusion in 2007–2008 (Jakobsdóttir et al., 2008; White et al., 2011), and beneath Askja volcano, attributed to melt migration (Soosalu et al., 2010; Key et al., 2011; Greenfield and White, 2015).

Shallow earthquakes cluster in three regions: (i) around the table mountain Herðubreið, assigned to the differential motion of the Askja and the Kverfjöll rift segments accommodated by bookshelf faulting (Green et al., 2014); (ii) around the northern part of the shield volcano Vaðalda; and (iii) at the southeastern corner of the caldera lake Öskjuvatn, a region of high geothermal activity, the source location of the landslide. This cluster at Öskjuvatn has been seen in seismic data since 1975 (Einarsson, 1991; Jakobsdóttir, 2008; Greenfield and White, 2015) and was hypothesised to be caused by hydrothermal circulation above a shallow magma body (Soosalu et al., 2010) or by thermal cracking and heat extraction in the crust (Einarsson, 1991).



Relocation of 86 earthquakes in this southeastern hydrothermal area at lake Öskjuvatn showed that the events are concentrated at depths between 2–4 km b.s.l. (Greenfield et al., in press). Furthermore, this study showed that the earthquakes were located along a line of 2 km length stretching from the fumarolic vents, i.e. the northern edge of the landslide source area, to the northwest. During the observation period of this study from 2009 to 2015, the earthquakes were randomly distributed in space and at depth with no clear trend over time, and the focal mechanisms did not show a distinct pattern in the years before the landslide.

### 2.3 Meteorology

The highlands of Iceland have a subarctic climate with short, cool summers and long, cold winters. In the Askja area, mean January temperatures are around  $-8^{\circ}\text{C}$  and mean July temperatures are usually around  $6^{\circ}\text{C}$  (Einarsson, 1984). The Vatnajökull icecap shields the central highlands from moisture coming from the southeast and precipitation rates of  $600\text{ mm yr}^{-1}$  are relatively low compared to the Icelandic coast (Einarsson, 1984). In winter, most precipitation falls as snow and extensive patches of snow usually last well into the summer months at the Askja central volcano. This was also the case in July 2014 (Helgason et al., 2014).

The area around the Askja central volcano experienced a period of warm weather in the middle of July 2014, with average daily temperatures between  $8\text{--}11^{\circ}\text{C}$  and maximum daily temperatures between  $12\text{--}15^{\circ}\text{C}$  (Fig. 2). The day of the landslide, 21 July, was one of the warmest of 2014 in the Icelandic highlands with temperatures around  $22^{\circ}\text{C}$ . The fair-weather period in mid-July 2014 was relatively dry but weather station Kárahnjúkar, 43 km east of Askja, recorded 9.3 mm of precipitation on 19 July and 8.7 mm on 20 July (Fig. 2). On the day of the landslide, the station recorded minor precipitation events with a total of 0.5 mm in the morning and over mid-day. These meteorological conditions with warm and wet weather in the days before the landslide increased the availability of water, due to snow melt promoted by high temperatures and rain on snow, which may have resulted in enhanced infiltration into the landslide body. This was facilitated by numerous cracks that had developed on top of the landslide mass a year before the failure (Fig. 3). Higher water content increases the pore pressure and, in turn, lowers the critical stress necessary to initiate slope failures (Iverson et al., 1997; Gaucher et al., 2015).

### 3 Seismic signal analysis

A network of 58 seismic stations was in place in the Icelandic highlands clustering around the Askja volcanic system from 2009 to 2015, to investigate the crustal structure and magma migration beneath the Askja central volcano. The stations were equipped with broadband to semi-broadband seismometers of the type Guralp CMG-6TDs (30 s – 100 Hz), CMG-ESPCDs (60 s – 100 Hz), and CMG-3Ts (120 s – 100 Hz) with Nanometrics Taurus data loggers, recording at 100 Hz sampling frequency. Based on data availability, the records of 52 stations were used in this study.



Coalescence Microseismic Mapping, CMM, was used to automatically detect, locate and classify crustal earthquakes in the Askja region (Drew et al., 2013). Between 21 June and 16 August 2014, twelve events with local magnitudes  $M_L < 2$  were on average detected per day by the whole network. In the days before the landslide, the crustal seismicity was within the background rate and on the day of the landslide the only event occurring within the Askja caldera was a  $M_L=0.5$  earthquake at 11 km depth, 1.5 km NE of the landslide source area at 15:15:19 UTC. Earthquakes occurring close to the surface and down to 5 km depth clustered in the southeastern corner of the Askja caldera beneath the landslide source area during the weeks before and after the landslide, with about two events per day.

### 3.1 High frequency seismic data analysis

To investigate the characteristics of the seismic signal of the landslide, we removed the instrument response, the mean and the trend, and band-pass filtered the signal between 1-45 Hz. We also computed spectrograms from the deconvolved vertical components of the seismic signals with time windows of 1.1 and 1.5 s and overlaps of 90%.

The high-amplitude short-period signals generated by the Askja landslide can be seen in the data of all stations of the network up to a distance of 110 km (station SKAF, south of Vatnajökull glacier). The seismic signal onset at the closest station MOFO, 3.5 km southeast of the landslide source area, was recorded at 23:24:05 UTC (Fig. 4) and started with a smooth increase in seismic ground velocities in the first 45 s. Amplitudes peaked 45 s and again 75 s after the first wave arrival with ground velocities of up to  $80 \mu\text{m s}^{-1}$  (Fig. 5b). Given that the amplitudes were generally higher for the horizontal components of the signal we attribute the signal to surface waves. The short-period signal lasted for about 130 s and the waveform has a symmetric, cigar-like shape. These characteristics of an emergent onset without clear *P* and *S* wave arrivals and no distinct peak amplitudes in the frequency bands  $>1$  Hz are characteristic of seismic signals generated by gravitational instabilities (Suriñach et al., 2005; Deparis et al., 2008; Dammeier et al., 2011; Burtin et al., 2013).

The spectrogram of station MOFO reveals that most energy was released within the first 2 min of the landslide until 23:26:00 UTC, with the frequencies between 1–4 Hz containing the largest part of the seismic energy. The spectrogram of the landslide has a triangular shape where the higher frequencies decrease more rapidly in energy over time (Fig. 4). This shape is common for landslides (Bottelin et al., 2014; Dammeier et al., 2015) and has been related to the fact that low frequencies attenuate slower than high frequencies (Aki, 1980). After these 2 min of persistent high seismic amplitudes and energies between 1–15 Hz, amplitudes and energies decayed rapidly in the subsequent 4 min, followed by 10 min during which seismic amplitudes decreased less rapidly. Approximately 40 min after the end of the high amplitude signals, the background noise level was re-established.

### 3.2 Landslide force history inversion of long-period signals

Long-period seismic waves radiated by landslides result from the cycle of unloading and reloading of the solid Earth (Fukao, 1995, Takei and Kumazawa, 1994). This broad loading cycle is produced by the bulk acceleration and deceleration of the



landslide mass (Okal, 1990). Long-period seismic signals (12.5–50 s, corresponding to frequencies of 0.02–0.08 Hz) were recorded for the Askja landslide at all stations of the network (station furthest away is LAUF, at 130 km distance, located SW of Vatnajökull glacier). As for the short-period signals, the long-period waves first arrived at station MOFO at 23:24:05 UTC and lasted for approximately 130 s. The onset of these long-period waves coincided with the arrival of the short-period waves.

Following the method developed by Ekström and Stark (2013) and Chao et al. (2016), we performed an inversion of the long-period landslide signals between 0.02–0.08 Hz, fitting synthetic waveforms to the data. This frequency range is suitable for the inversion as higher frequencies would be affected by local-scale structures and inaccuracies in the velocity model, and lower frequencies have insufficient signal-to-noise ratios. We tested frequency ranges of 0.02–0.05 Hz, 0.02–0.08 Hz and 0.04–0.08 Hz to analyse the sensitivity of the inversion to the chosen frequency range. For the inversion, we used the 1-D velocity model for the Askja region developed by Mitchell et al. (2013) and the record of eleven broadband stations of the seismic network (see inset of Fig. 5). We selected those stations because their data has high signal-to-noise-ratio and they were equipped with CMG-ESPCDs or CMG-3Ts instruments capable of recording frequencies between 0.0167–100 Hz, low enough for the inversion.

The results of our inversion show that the unloading forces due to the accelerating mass of the landslide are oriented towards the SE. In turn, the reloading forces due to the decelerating and depositing mass of the landslide strike to the NW. These directions are in agreement with the NW-directed propagation path of the landslide that we inferred from direct field observations of the landslide source and deposition area in August 2015. The inversion also gives the location history of the centre of the landslide mass (Fig. 5) moving to the NW in about 130 min. From the inversion, we obtained a total horizontal displacement of  $1260 \pm 250$  m and a vertical displacement of  $430 \pm 300$  m for the centre of the landslide mass.

The inversion results give  $7\text{--}16 \times 10^{10}$  kg of mobilised mass and the potential energy released during this landslide is estimated to be  $8.2\text{--}51.5 \times 10^{13}$  J. Assuming an average density of  $2000 \text{ kg m}^{-3}$ , representative of typical values for highly fractured and hydrothermally altered Pleistocene hyaloclastites and Holocene basaltic lava flows (Moore 2001), the collapsed volume was  $35\text{--}80 \times 10^6 \text{ m}^3$ . This is in the range of values estimated from field observations and bathymetric surveys of the lake, giving  $12\text{--}50 \times 10^6 \text{ m}^3$  for the landslide volume (Hoskuldsson et al., 2015; Saemundsson et al., 2015; Gylfadóttir et al., 2017). Sonar investigations detected the deposits of the landslide in the lake as far as 2000 m away from the entry point of the material into the water (Hoskuldsson et al., 2015) and a calculation of the landslide volume deposited in the lake based on the rise of the water level is  $10 \times 10^6 \text{ m}^3$  (Gylfadóttir et al., 2017). This is less than half the total landslide volume, consistent with our finding that the centre of mass came to rest almost at the lakeshore (Fig. 5).



#### 4 Tremor

When inspecting the deconvolved and band-pass filtered high-frequency data (1–45 Hz) we found that the background noise level started to rise about 30 min before the high-energy landslide signal, at approximately 22:55 UTC. This increase of the background amplitudes is visible in the stations up to 30 km away from the landslide area. For the nearest station MOFO, the seismic amplitudes were up to three times higher than the background at 23:17 UTC, 7 min before the onset of the high-energy landslide signal. This was followed by an amplitude drop to values slightly below the background 2 min before the onset of the landslide signal (Fig. 6).

In the spectrograms, the increasing amplitudes are shown as a continuous, harmonic signal with a fundamental frequency of 2.5 Hz and overtones at 5 and 7.5 Hz. Due to these characteristics, we call this signal ‘tremor’ in the following. At about 23:14 UTC, the spectral content of the tremor started to change and both up and down gliding frequency bands can be observed simultaneously (Fig. 6a). Concurrent with the amplitude drop, the gliding spectral lines stopped at about 23:22 UTC and a period of 2 min of quiescence can be seen in the spectrograms before the high-energy signal of the landslide starts. As the gliding includes the same frequency bands in the data of all stations showing the tremor, we conclude that the nature of the signal is a source property rather than a site or wave propagation effect. To test this, we stacked the signals of the eight closest stations operating at the time of the tremor (DREK, GODA, HOTT, JONS, KLUR, MOFO, STAM, VADA, see inset of Fig. 7 for locations) and computed the mean fundamental frequency. The maximum standard deviation to this mean of 2.5 Hz for the eight closest stations is only 0.3 Hz.

Seismic amplitudes for the Askja landslide tremor are higher for the horizontal components than for the vertical component, which implies that the signal is dominated by surface waves. In contrast to the seismic signal of the landslide that also contains long-period seismic waves, the tremor is confined to frequencies above 1 Hz.

##### 4.1 Tremor localisation

For a rough estimation of the tremor location and to check whether it is not only temporally but also spatially correlated with the landslide, we computed the amplitude ratio of 10 min of background seismic noise to 1 min of the tremor starting at 23:17 UTC for the vertical components of all stations of the network. The amplitude ratio is highest at the stations closest to the source area of the landslide and decays the further away the station is located from Lake Öskjuvatn. However, we note that this decay has an elliptical outline with a long axis oriented NE-SW, parallel to the orientation of the general structural trends at the Askja volcanic system, which are probably responsible for seismic wave attenuation effects.

To further refine the location of the tremor, we used the migration procedure of Burtin et al. (2013) to locate the tremor signal on a DEM grid. This statistical approach assigns a probability to each grid point that it is the source of the signal based on cross-correlation of the waveforms at different stations. We used 21 stations for the location that showed the gliding spectral lines in the spectrograms and a DEM with a grid spacing of 100×100 m. With the migration, we found that the tremor signal most likely located at the southeastern shore of the caldera lake, where fumaroles are the surface expression of





the hydrothermal system (Fig. 7). This is the northern corner of the landslide source area. The time series of the location for 30 min before the landslide showed that the likely tremor location only changed of the order of a few 100 m during this time period. We tested the influence of the seismic wave velocity on the results by changing this parameter in the migration procedure between 500 and 3700 m s<sup>-1</sup>. The best-fit locations for the different wave velocities differ up to 500 m from each other but remain at the southeastern lakeshore.

#### 4.2 Nature of the precursory tremor

If the individual events of a repeatable, non-destructive stationary source mechanism occur so frequently that they cannot be distinguished and merge into a continuous signal, then seismic tremor results (Neuberg, 2000; Powell and Neuberg, 2003). The term tremor describes a continuous seismic signal resembling an irregular sinusoid that can last for minutes up to days or even weeks (McNutt, 1992). Tremor has been observed in a variety of settings including volcanically active and glaciated regions. Possible source mechanisms for tremor that have been put forward include: (i) fluid-flow-induced excitation and oscillations of volcanic conduit walls (Julian, 1994; Hellweg, 2000; Rust et al., 2008; Matoza et al., 2010; Corona-Romero et al., 2012; Unglert and Jellinek 2015); (ii) excitation and resonance of fluid-filled cracks or pipes with open or closed ends (Chouet, 1985, 1986, 1988; Benoit and McNutt, 1997; Jousset et al., 2003; Neuberg, 2006; Jellinek and Bercovici, 2011; Rööslü et al., 2014; Sturton and Walter et al., 2015);, (iii) bubble growth or collapse due to hydrothermal boiling of groundwater (Leet, 1988; Kedar et al., 1998; Cannata et al., 2010); and (iv) continuously repeating processes such as rock and ice deformation and frictional faulting (Neuberg, 2000; Powell and Neuberg, 2003; Dmitrieva et al., 2013; Hotovec et al., 2013; Lipovsky and Dunham, 2015; see also reviews by McNutt, 1992 and Konstantinou and Schlindwein, 2003).

Brace and Byerlee (1966) proposed that tremor can occur when stick-slip motion on a fault generates frequent small earthquakes. The hypothesis of stick-slip motion creating tremor on a sliding plane is supported by geodetic measurements in the field (MacAyeal et al., 2008; Martin et al., 2010; Winberry et al., 2013), by numerical models (Nadeau and Johnson, 1998; Lipovsky and Dunham, 2016) and by laboratory friction experiments (McLaskey and Glaser, 2011; Zigone et al., 2011). Hence, tremor at active plate boundaries is interpreted as a superposition of many low-frequency earthquakes representing slip on faults (Shelly et al., 2007, 2006).

Stick-slip motion can also occur on the sliding plane of a surface mass movement. This has been proposed to create tremor associated with the movement of landslides (Yamada et al., 2016) and ice-rock avalanches (Caplan-Auerbach et al., 2004, Huggel et al., 2008), with the sliding of ice-sheets and glaciers (Caplan-Auerbach and Huggel, 2007; Wiens et al., 2008; Winberry et al., 2013; Allstadt and Malone, 2014; Helmstetter et al., 2015; Lipovsky and Dunham, 2016), and with iceberg collisions (MacAyeal et al., 2008, Martin et al., 2010).

Seismic tremor often shows sharply peaked spectra with a fundamental frequency and several overtones and is then called harmonic tremor (McNutt, 2005). The phenomenon of systematically varying frequencies of the tremor spectral peaks with time is known as gliding (McNutt, 2005). For stick-slip source processes of the tremor, gliding of the frequency bands has been attributed to (i) a change in the trigger frequency, i.e. in the repetition time of a stationary source such as stick-slip



earthquakes (Lockner et al., 1991; Neuberg 2000; Dmitrieva et al., 2013; Hotovec et al., 2013), or (ii) a change in the geometrical properties of the stick-slip sliding plane (Lipovsky and Dunham, 2016).

Considering that a voluminous landslide was set in motion, we propose that the tremor signal before the main landslide failure at the Askja caldera is most likely caused by stick-slip motion on frictional unstable patches in the lead up to stable sliding and the large-scale displacement of the landslide bulk. We envisage the stick-slip planes to be located at the base or at the edges of the landslide, developing along heterogeneities such as the lithological contact between the hyalocastites and the 1923 Suðurbotnahraun lavas, and pre-existing material heterogeneities within the hydrothermally altered hyaloclastites. Stick-slip sliding taking place at the base of the landslide rather than predominately within it would result in a better coupling and thus higher energy transmission to the ground. This explains why the tremor can be observed over 30 km away from the landslide source region.

The tremor signal before the Askja landslide is harmonic and individual earthquakes cannot be distinguished, even at its onset. We deduce that the individual, repeating stick-slip events occurred very close together in time from the start of instability. This is in contrast to other seismic observations of landslides where individual stick-slip events could be distinguished before the main failure (Yamada et al., 2016). However, in that case, the source-to-station distance was <1 km whereas our closest station is 3.5 km from the landslide source area. Thus, we argue that individual stick-slip events before the Askja landslide may not have been detectable kilometres away and that the events must occur already very close in time and transmit enough energy that they can be seen from a longer distance, likely as a continuous tremor signal.

Also in line with stick-slip motion of the landslide are the observations that cracks in the head wall of the landslide started to open after 2011 (Helgason et al., 2014) and that numerous cracks had developed at the surface of the landslide mass a year before the failure (Fig. 3). This implies that the failure planes bounding the landslide developed years before the bulk movement of the landslide mass and just needed to be activated. The warm and wet weather, promoting pore pressure increase in July 2014 may have played an important role in this. Slight increases in pore water pressure can induce stick-slip motion, as has been observed on blocks of a seasonally active landslide in the French Alps (Genuchten and Rijke, 1989).

Although an accelerating cracking process might also be a possible tremor source before the Askja landslide, we argue against it for the following reasons. To create harmonic tremor with overtones as we observe it, individual events must have very similar waveforms and likely occur at the same location, for instance at asperities of sliding patches. In contrast, cracking events are often distributed over a wider area and hence change their waveforms (Lockner et al., 1991; Ito and Enoki, 2007). In addition, the large distance of more than 3.5 km from tremor source to seismic receiver limits the recording of high-energy cracking events in our seismic network.

An eye catching aspect of the Askja tremor is the occurrence of up-gliding and down-gliding, followed by a quiet period, 2 min before the high-energy signals of the main landslide can be seen in the seismic data (Fig. 6). This disappearance of the tremor signal shortly before the landslide is consistent with the theoretical prediction of a transition from stick-slip to stable sliding at high loading rates, which occurs aseismically (Gomberg et al., 2011). This would imply that the landslide mass had already started to move before the high-energy signals emerged in the seismic data. As the tremor before the quiet period



consists of synchronous up- and down-gliding frequencies we infer that at least two sources, i.e. stick-slip sliding patches, were active at the same time. As one sliding patch decelerated producing down-gliding spectral lines another patch speeded up producing up-gliding spectral lines. This accelerating patch eventually slips aseismically and then fails catastrophically. In contrast, if we assume instead two resonators as tremor sources, the quiet period before the main landslide can only be explained if the resonators stopped emitting seismic signals. However, we cannot imagine a physical explanation for that.

### 4.3 Tremor modelling

We used the numerical model of small repeating earthquakes developed by Lipovsky and Dunham (2016) to reproduce the seismic signal created by the tremor before the Askja landslide. This model was originally developed to describe repeating basal earthquakes during the stick-slip motion of an Antarctic ice stream (Lipovsky and Dunham 2017). The force balance in this model is between elastic stresses, including elastic wave propagation, and an interfacial strength set by rate-and-state friction. We compute synthetic seismograms from these simulations. As both up- and down-gliding spectral lines occur simultaneously in the Askja dataset, we infer that more than one source was active at the same time, each producing tremor. Hence, we use two simulations. In the first, the repeat time between the stick-slip events decreases with time, and in the second, the inter-event time increases with time.

This numerical model requires several parameters to be specified. First, the interface normal stress must be prescribed, and for this value we use an overburden stress equal to a landslide thickness of 30 m, consistent with a previous work (Gylfadóttir et al. 2017). This number is a simplification as we do not expect the landslide to be of constant thickness throughout the entire sliding body. Furthermore, three frictional parameters,  $a$ ,  $b$ , and  $d_c$ , described below, must be prescribed. These values are typically considered to be material properties and are commonly measured in laboratory experiments (Marone, 1998). For these parameters, we use typical values for crustal rocks (Table 1).

By matching the synthetic and observed seismograms we match two prominent observations. First, we reproduce the aseismic period immediately before the main landslide failure (Fig. 8). The termination of the spectral lines corresponds to the transition to aseismic sliding. Second, we find that the up-gliding of the spectral tremor lines can be produced by stick-slip earthquakes occurring with increasing frequency (decreasing repeat time  $T$ ) on a region of the sliding interface with a radius of 45 m (Fig. 8b). Down-gliding, in contrast, occurs when stick-slip cycles happen with decreasing frequency (increasing repeat time  $T$ , Fig. 8a). We now describe the mechanical basis of these two observations.

The aseismic-seismic transition is a central feature of sliding under rate-and-state friction (Rice et al., 2001; Lipovsky and Dunham, 2016). This transition is commonly expressed as a critical patch size  $R_c$ , defined such that with all other parameters held constant, a given interface will only experience stick-slip oscillations if  $R < R_c$ , with  $R_c$  defined as

$$R_c = \frac{d_c G}{(b-a)\sigma - \eta v_0} \quad (1).$$

In this expression,  $\sigma$  is the normal stress and  $G$  is the shear modulus,  $d_c$  is the frictional state evolution distance,  $a$  is the magnitude of transient peak strengthening during step loading,  $b$  is the magnitude of strength change between peak strength



and steady state,  $\eta = \rho c_s$  is the shear wave impedance with density  $\rho$  and shear wave speed  $c_s$ , and  $v_0$  is the nominal loading velocity. The parameter (b-a) must be positive for stick-slip cycles to occur; an interface with this property is called rate weakening.

Under rate-and-state friction, a change in the repeat time  $T$  of the stick-slip events may occur for a number of reasons. Near  
 5 the transition between steady and stick-slip sliding,  $T$  scales approximately as (Lipovsky and Dunham 2016, 2017),

$$T/T_c = R/R_c \quad (2)$$

where  $T_c$  is the lowest achievable repeat time.

$$T_c = 2\pi \sqrt{\frac{a}{(a-b)} \frac{dc}{v_0}} \quad (3).$$

Assuming that all material parameters remain constant, it follows from Eq. (2) that the two ways to change the recurrence  
 10 frequency are to change the patch size, or the loading velocity. It is our conclusion at this time that the seismic data are not strictly able to discern between these two alternative explanations at this time. Nevertheless, given the ensuing acceleration associated with the Askja landslide, we favour the simplest explanation of a changing sliding velocity. We suggest the following testable corollary of this interpretation.

We interpret the up-gliding and down-gliding tremor as due to increasing and decreasing sliding velocity at two different  
 15 sites along the landslide interface, respectively. This suggests large-scale straining of the landslide material. If the two patches are separated in space by a distance  $dx$ , then this implies that the material between the patches are experiencing a net longitudinal strain acceleration in the moments before the landslide,

$$\ddot{\epsilon}_{xx} \approx \frac{\dot{v}_1 - \dot{v}_2}{dx} \quad (4).$$

If  $dx$  is about 1 km, then this implies a strain acceleration on the order of  $10^{-8} \text{ (s}^{-1}) \text{ min}^{-1}$ . Tremor took place for  
 20 approximately two hours before the landslide, suggesting that large strains on the order of  $10^{-2}$  accumulated during this time. These strains could in principal be observed with sufficiently high spatial resolution geodetic observations.

The stress drop in each stick-slip event is given by

$$\Delta\tau = \alpha G \frac{u}{R} \quad (5)$$

where  $\alpha$  is a geometrical constant usually taken to be  $7/16 \pi \sim 1.37$ , and  $u$  is the slip in each event. With the parameters of  
 25 our best-fit model,  $u=0.24$  mm,  $R=40$  m, and  $G=7$  GPa, we calculated a stress drop of 56.2 kPa. The scalar moment is  $M_0=8.4 \times 10^9$  Nm, which is equivalent to a moment magnitude  $M_w=0.58$ . This is comparable to the moment magnitudes of most of the earthquakes recorded in the hydrothermal system below the southeastern lake shore at Öskjuvatn that are usually smaller than  $M_L \sim 1$  (Greenfield et al., in press).



## 5 Afterslides

During 8 hours after the main landslide, several other high-amplitude short-period signals of much lower amplitude were recorded (for example, at 23:41:10 UTC, Fig. 4). Their waveforms are cigar-shaped with dominant frequencies of about 1–2 Hz. The signals are only visible at frequencies >1 Hz and a force history inversion of low-frequency signals is not possible.

5 These events lasted between a few seconds and a minute and have characteristics such as emergent onsets, slowly decaying tails, and triangularly shaped spectrograms that have been described elsewhere from slope failures (Dammeier et al., 2011; Burtin et al., 2013; Chen et al., 2013). We attribute these signals to smaller slope failures that occurred after the main landslide. Following the nomenclature for earthquakes with the main shock and subsequent, smaller aftershocks happening in the same area, we here introduce the term afterslides for smaller mass movements occurring after a large landslide on the  
10 same landslide scar.

We used the same migration procedure of Burtin et al. (2013) that we applied for the tremor localisation to locate the seismic signals of the afterslides on a DEM grid. Their locations cluster at the destabilised walls from which the main landslide originated. The afterslides get less and less frequent and smaller in amplitude during the 8 hours following the main landslide (Fig. 9).

## 15 6 Discussion

### 6.1 Dynamics of the landslide sequence from high- and low-frequency signals

Combining seismic data analysis and field observations reported in the literature and made during a field campaign in August 2015, we were able to summarise the factors that lead to the landslide and describe the precursory tremor, the landslide and the subsequent rock falls in detail.

20 Crack opening started years before the landslide at the head wall of the slide as documented in pictures taken from 2011 onward (Helgason et al., 2014). The warm weather with a number of precipitation events in July 2014 further promoted this crack opening by bringing moisture to the Askja caldera and increasing the snowmelt, both giving rise to higher pore pressure. On 21 July 2014, at about 22:55 UTC, that is half an hour before the main failure, the landslide mass slowly started to move downslope. This is evidenced by the seismic record of 38 stations located up to 30 km away from the Askja caldera  
25 that show a complex harmonic tremor signal with a fundamental frequency of 2.5 Hz and several overtones. The activated spectral lines change their frequency content during an 8 min period starting at 23:14 UTC. Synchronous up- and down-gliding of the frequency bands indicate that several sliding planes at the base of the landslide experienced stick-slip motion at the same time. As the waveforms of the stick-slip earthquakes have to be similar for their merged signal to be visible as harmonic tremor with overtones we envisage this to happen because the moving patches gradually slide over harder  
30 obstacles at their base.



The stick-slip sliding accelerated to an aseismic, stable sliding period, 2 min before the bulk landslide mass failed catastrophically. Based on combined inspection of the high- and low-frequency signals generated by the Askja landslide, we distinguish three phases of landslide motion: initiation, propagation and termination (Hibert et al., 2014; Chao et al., 2016). The initiation phase of the landslide started immediately before surface waves arrived at about 23:24:05 UTC at the nearest station. The landslide force history inversion shows a sharp increase in the accelerating force during the first 30 sec of the landslide signal generated by the onset of motion of the landslide's bulk mass. The high-frequency signals show an emergent onset during these first 30 sec. They reach maximum amplitudes about 45 sec after the signal onset, which coincides with lower acceleration and the transition to decelerated motion in the force history inversion of the propagation phase. We infer from this lag time in the high-frequency signal that the main slope failure along the southeastern caldera wall was a single, large event, starting with aseismic sliding of a relatively coherent mass that gradually fragmented during down-slope acceleration (Allstadt, 2013; Hibert et al., 2015). In this interpretation, the high-frequency signals are caused by the momentum exchanges of block impacts, and frictional processes within the moving slide and along its boundaries, especially when the moving mass traverses small-scale topographic features on the sliding base (cf. Dammeier et al., 2011; Allstadt, 2013). These multiple sources, along with the diversity of propagating waves, are responsible for the multiple amplitude pulses and the lack of a clear maximum of the seismic amplitudes in the higher frequencies (Deparis et al., 2008; Dammeier et al., 2011). The deceleration phase of the landslide force history inversion lasts for about 70 sec, a period during which the high-frequency amplitudes also gradually decline. This termination phase of the landslide is associated with material deposition at the shore but also into Lake Öskjuvatn.

From the landslide force history inversion, we calculate that about  $30\text{--}80 \times 10^6 \text{ m}^3$  of hyaloclastitic material was involved in the slide and about  $10 \times 10^6 \text{ m}^3$  entered Lake Öskjuvatn creating a tsunami (Gylfadóttir et al., 2017). As a result of the removal of overlying mass, the hydrothermal system below the landslide source area was depressurised and a steam cloud rose above the caldera (Helgason et al., 2014).

During the 8 hours after the main landslide, subsequent small slope failures occurred at the destabilised caldera walls. The rolling, jumping, colliding and impacting blocks created seismic signals with emergent onsets, cigar-shaped envelopes (Dammeier et al., 2011; Allstadt, 2013; Hibert et al., 2015; Moretti et al., 2015) and of higher seismic amplitudes than the background level at the stations closest to the Askja caldera. Such a chain-reaction with subsequent slope collapses is not uncommon after landslides (Iverson et al., 2015). Similar to earthquakes and their aftershocks that occur less frequently and with smaller amplitudes with time after the main shock (Omori, 1894, Gutenberg and Richter, 1956), we observe a decay in the size and frequency of the afterslides.

## 6.2 Tremor as early-warning sign of landslide failure

Through analysis of the seismic signal of the tremor preceding the Askja landslide we are able to show that localised stick-slip motion may have culminated in large-scale slope failure. A well-positioned network of seismic stations located close to



and a few kilometres away from the slope instability should be able to detect precursory tremors in other cases as well. Consequently, with rapid detection, tremor signals could be used in an early-warning system for landslides that are activated by stick-slip motion. Many voluminous slope failures start as slow-moving landslides (Palmer 2017) and may have stick-slip behaviour; an early-warning system based on seismic signals of precursory slope activity could be widely used. Some

5 already monitored slow-moving landslides show displacement rates that scale with the seismicity rates of cracks and stick-slip tremor signals (Tonnellier et al., 2013, Vouillamoz et al., 2017) and could serve as test sites.

To implement seismic observations of precursory tremor signals into an early-warning system, the seismic data stream needs to be analysed in real time or near-real time by a fast and reliable algorithm. Machine-learning methods could form the basis for such an algorithm as they are a powerful and promising tool to detect and classify signal classes, also of precursory slope

10 activity, in seismic data (Hammer et al., 2012; Esposito et al., 2013; Zeckra et al., 2015). Other anticipative signals of natural gravity-driven instabilities such as those of cracking could also be detected and identified in this way. Cracking and fracturing signals have been identified in seismic data before cliff collapses (Amitrano et al., 2005; Zeckra et al., 2015), slope instabilities (Sima, 1986; Kolesnikov et al., 2003; Dixon et al., 2015; Faillettaz et al., 2016; Yamada et al., 2016), and break-off of hanging glaciers (see review by Faillettaz et al., 2015).

15 As seismic instruments sample at a very high rate, usually  $>50$  Hz, they can complement other monitoring techniques that acquire data less frequently and often only during campaigns, like airborne and satellite-based remote sensing techniques. Furthermore, seismic techniques are a non-invasive method that can detect signals over several kilometres in any direction. The advantage over other ground-based instrumentations of unstable slopes, for instance with strain meters, is a higher level of safety as the seismic stations do not need to be installed right on or very close to the unstable part. They also provide full

20 monitoring of the surrounding landscape, from the slope, over the catchment area and up to the regional scale.

Up to date, monitoring of landslides has focused mainly on individual localities with instrumentation inside or very close to the sliding body. At the Super-Sauze (France), the Valoria (Italy) and the Pechgraben (Austria) slow-moving landslides, several event classes have been detected seismically (Walter et al., 2012; Tonnellier et al., 2013). Those classes include signals produced by material bending, shearing, compression and creeping, brittle failure and fissure opening, slip at the

25 bedrock interface and at the edges of the slide, rockfalls and debris flows. However, regional scale landslide monitoring with a seismic network has only been attempted on a few occasions (Burtin et al., 2013; Hibert et al., 2014) and the challenge persists to detect landslide signals in a continuous seismic data stream in real to near-real time (Dammeier et al., 2016; Manconi et al., 2016; Chao et al., 2017). But the inter-station distances of those networks are often too large to detect any precursory slope activity. A denser network with stations at  $<3$  km distance would be needed to pick up precursory signals of

30 stick-slip motion or cracking before large slope failures.



## 7 Conclusions

We analysed seismic data from a voluminous landslide and its precursory tremor that occurred at the southeastern shore of the caldera lake Öskjuvatn of the Askja central volcano in the Icelandic Highlands on 21 July 2014. The seismic data is of exceptional high quality because (i) the 58 stations were centred around the Askja caldera, and (ii) anthropogenic noise sources are far away. We performed a detailed analysis of the seismic data that showed that the short-period signals of the landslide mainly consist of surface waves, which arrived at the closest station at 23:24:05 UTC and lasted for about 130 s. The seismic signal of the Askja landslide is characteristic of voluminous slope failures with an emergent onset without clear  $P$  and  $S$  wave arrivals and a cigar-shaped envelope. Inversion of the long-period signals of the landslide reveals that the bulk mass of  $30\text{--}80\times 10^6\text{ m}^3$  propagated to the northwest starting at the caldera ring fault at the southeastern shore of Lake Öskjuvatn, which is consistent with field observations.

The excellent data quality enabled us to detect harmonic tremor commencing about 30 min before the landslide in the data of the stations up to 30 km away from the landslide source area. We attribute the simultaneously up and down gliding spectral lines of the tremor to be created by accelerating and decelerating movement of two sliding planes, which each produce repeated stick-slip earthquakes. The transition from stick-slip to stable sliding is marked by a seismically quiet period of 2 min before the bulk landslide mass failed catastrophically. We emphasise the utility of seismic networks to detect and characterise not only landslides but also the precursory signals that might otherwise go unnoticed. This is of utmost importance for sites with a high hazard potential and encourages the development of early-warning systems based on seismic data for monitoring slope failures.

## Acknowledgements

Seismometers were provided by the Natural Environmental Research Council (NERC) SEIS-UK under loans 968 and 1022. We would like to thank the Icelandic Meteorological Office for making the weather data available. The field campaign in summer 2015 was financially supported by an expedition fund of the Helmholtz Centre Potsdam GFZ and T. Witt, T. Walter, D. Müller, B. Steinke, and Á. Höskuldsson are thanked for their support in the field. Some figures were created with the help of GMT, Generic Mapping Tools, developed by Wessel et al. (2013).

## References

- Acocella, V., Di Lorenzo, R., Newhall, C. and Scandone, R.: 2015, An overview of recent (1988 to 2014) caldera unrest: Knowledge and perspectives, *Reviews of Geophysics* **53**(3), 896–955.
- Aki, K.: 1980, Attenuation of shear-waves in the lithosphere for frequencies from 0.05 to 25 Hz, *Physics of the Earth and Planetary Interiors* **21**(1), 50–60.





- Allstadt, K.: 2013, Extracting source characteristics and dynamics of the August 2010 Mount Meager landslide from broadband seismograms, *Journal of Geophysical Research: Earth Surface* **118**(3), 1472–1490.
- Allstadt, K. and Malone, S. D.: 2014, Swarms of repeating stick-slip icequakes triggered by snow loading at Mount Rainier volcano, *Journal of Geophysical Research: Earth Surface* **119**(5), 1180–1203.
- 5 Amitrano, D., Grasso, J. R. and Senfaute, G.: 2005, Seismic precursory patterns before a cliff collapse and critical point phenomena, *Geophysical Research Letters* **32**, L08314, doi:10.1029/2004GL022270.
- Benoit, J. P. and McNutt, S. R.: 1997, New constraints on source processes of volcanic tremor at Arenal Volcano, Costa Rica, using broadband seismic data, *Geophysical Research Letters* **24**(4), 449–452.
- Bottelin, P., Jongmans, D., Daudon, D., Mathy, A., Helmstetter, A., Bonilla-Sierra, V., Cadet, H., Amitrano, D., Richefeu,  
10 V., Lorier, L., Baillet, L., Villard, P. and Donzé, F.: 2014, Seismic and mechanical studies of the artificially triggered rockfall at Mount Néron (French Alps, December 2011), *Natural Hazards and Earth System Sciences* **14**, 3175–3193.
- Brace, W. and Byerlee, J.: 1966, Stick-slip as a mechanism for earthquakes, *Science* **153**(3739), 990–992.
- Brodsky, E. E., Gordeev, E. and Kanamori, H.: 2003, Landslide basal friction as measured by seismic waves, *Geophysical Research Letters* **30**(24), 2236, doi:10.1029/2003GL018485.
- 15 Burtin, A., Hovius, N., Milodowski, D. T., Chen, Y.-G., Wu, Y.-M., Lin, C.-W., Chen, H., Emberson, R. and Leu, P.-L.: 2013, Continuous catchment-scale monitoring of geomorphic processes with a 2-D seismological array, *Journal of Geophysical Research: Earth Surface* **118**(3), 1956–1974.
- Cannata, A., Di Grazia, G., Montalto, P., Ferrari, F., Nunnari, G., Patanè, D. and Privitera, E.: 2010, New insights into banded tremor from the 2008–2009 Mount Etna eruption, *Journal of Geophysical Research: Solid Earth* **115**, B12318,  
20 doi:10.1029/2009JB007120.
- Caplan-Auerbach, J., Prejean, S. G. and Power, J. A.: 2004, Seismic recordings of ice and debris avalanches of Iliamna Volcano (Alaska), *Acta Vulcanologica* **16**(1/2), 9.
- Caplan-Auerbach, J. and Huggel, C.: 2007, Precursory seismicity associated with frequent, large ice avalanches on Iliamna volcano, Alaska, USA, *Journal of Glaciology* **53**(180), 128–140.
- 25 Chao, W.-A., Zhao, L., Chen, S.-C., Wu, Y.-M., Chen, C.-H. and Huang, H.-H.: 2016, Seismology-based early identification of dam-formation landquake events, *Scientific Reports* **6**, 19259.
- Chao, W.-A., Wu, Y.-M., Zhao, L., Chen, H., Chen, Y.-G., Chang, J.-M. and Lin, C.-M.: 2017, A first near real-time seismology-based landquake monitoring system, *Scientific Reports* **7**, 43510.
- Chen, C.-H., Chao, W.-A., Wu, Y.-M., Zhao, L., Chen, Y.-G., Ho, W.-Y., Lin, T.-L., Kuo, K.-H. and Chang, J.-M.: 2013, A  
30 seismological study of landquakes using a real-time broad-band seismic network, *Geophysical Journal International* **194**, 885–898.
- Chouet, B.: 1985, Excitation of a buried magmatic pipe: a seismic source model for volcanic tremor, *Journal of Geophysical Research: Solid Earth* **90**(B2), 1881–1893.



- Chouet, B.: 1986, Dynamics of a fluid-driven crack in three dimensions by the finite difference method, *Journal of Geophysical Research: Solid Earth* **91**(B14), 13967–13992.
- Chouet, B.: 1988, Resonance of a fluid-driven crack: Radiation properties and implications for the source of long-period events and harmonic tremor, *Journal of Geophysical Research: Solid Earth* **93**(B5), 4375–4400.
- 5 Corona-Romero, P., Arciniega-Ceballos, A. and Sánchez-Sesma, F.: 2012, Simulation of lp seismic signals modeling the fluid–rock dynamic interaction, *Journal of Volcanology and Geothermal Research* **211**, 92–111.
- Dammeier, F., Moore, J. R., Haslinger, F. and Loew, S.: 2011, Characterization of alpine rockslides using statistical analysis of seismic signals, *Journal of Geophysical Research: Earth Surface* **116**, F04024, doi:10.1029/2011JF002037.
- Dammeier, F., Guilhem, A., Moore, J. R., Haslinger, F. and Loew, S.: 2015, Moment tensor analysis of rockslide seismic  
10 signals, *Bulletin of the Seismological Society of America* **105**(6), 3001–3014.
- Dammeier, F., Moore, J. R., Hammer, C., Haslinger, F. and Loew, S.: 2016, Automatic detection of alpine rockslides in continuous seismic data using hidden Markov models, *Journal of Geophysical Research: Earth Surface* **121**(2), 351–371.
- De Angelis, S. and McNutt, S. R.: 2007, Observations of volcanic tremor during the January–February 2005 eruption of Mt. Veniaminof, Alaska, *Bulletin of Volcanology* **69**(8), 927–940.
- 15 de Zeeuw-van Dalfsen, E., Rymer, H., Sturkell, E., Pedersen, R., Hooper, A., Sigmundsson, F. and Ófeigsson, B.: 2013, Geodetic data shed light on ongoing caldera subsidence at Askja, Iceland, *Bulletin of Volcanology* **75**(5), 1–13.
- DeMets, C., Gordon, R. G., Argus, D. F. and Stein, S.: 1994, Effect of recent revisions to the geomagnetic reversal time scale on estimates of current plate motions, *Geophysical Research Letters* **21**(20), 2191–2194.
- Deparis, J., Jongmans, D., Cotton, F., Baillet, L., Thouvenot, F. and Hantz, D.: 2008, Analysis of rock-fall and rock-fall  
20 avalanche seismograms in the French Alps, *Bulletin of the Seismological Society of America* **98**(4), 1781–1796.
- Dietze, M., Turowski, J. M., Cook, K. L. and Hovius, N.: 2017, Spatiotemporal patterns and triggers of seismically detected rockfalls, *Earth Surface Dynamics Discussion*, in review, doi:10.5194/esurf-2017-20.
- Dixon, N., Spriggs, M., Smith, A., Meldrum, P. and Haslam, E.: 2015, Quantification of reactivated landslide behaviour using acoustic emission monitoring, *Landslides* **12**(3), 549–560.
- 25 Dmitrieva, K., Hotovec-Ellis, A. J., Prejean, S. and Dunham, E. M.: 2013, Frictional-faulting model for harmonic tremor before Redoubt Volcano eruptions, *Nature Geoscience* **6**(8), 652–656.
- Drew, J., White, R. S., Tilmann, F. and Tarasewicz, J.: 2013, Coalescence microseismic mapping, *Geophysical Journal International* **195**(3), 1773–1785.
- Einarsson, M.: 1984, Climate of Iceland, in H. van Loon (ed.), *World Survey of Climatology: 15: Climates of the Oceans*,  
30 Elsevier, Amsterdam, pp. 673–697.
- Einarsson, P.: 1991, Earthquakes and present-day tectonism in Iceland, *Tectonophysics* **189**(1), 261–279.
- Ekström, G. and Stark, C. P.: 2013, Simple scaling of catastrophic landslide dynamics, *Science* **339**(6126), 1416–1419.



- Esposito, A. M., D'Auria, L., Giudicepietro, F., Peluso, R. and Martini, M.: 2013, Automatic recognition of landslides based on neural network analysis of seismic signals: an application to the monitoring of Stromboli volcano (Southern Italy), *Pure and Applied Geophysics* **170**(11), 1821–1832.
- Faillettaz, J., Funk, M. and Vincent, C.: 2015, Avalanching glacier instabilities: Review on processes and early warning perspectives, *Reviews of Geophysics* **53**(2), 203–224.
- Faillettaz, J., Or, D. and Reiweger, I.: 2016, Codetection of acoustic emissions during failure of heterogeneous media: New perspectives for natural hazard early warning, *Geophysical Research Letters* **43**(3), 1075–1083.
- Favreau, P., Mangeney, A., Lucas, A., Crosta, G. and Bouchut, F.: 2010, Numerical modeling of landquakes, *Geophysical Research Letters* **37**, L15305, doi: 10.1029/2010GL043512.
- 10 Fukao, Y.: 1995, Single-force representation of earthquakes due to landslides or the collapse of caverns, *Geophysical Journal International* **122**(1), 243–248.
- Gaucher, E., Schoenball, M., Heidbach, O., Zang, A., Fokker, P. A., van Wees, J.-D. and Kohl, T.: 2015, Induced seismicity in geothermal reservoirs: A review of forecasting approaches, *Renewable and Sustainable Energy Reviews* **52**, 1473–1490.
- Gomberg, J., Schulz, W., Bodin, P. and Kean, J.: 2011, Seismic and geodetic signatures of fault slip at the Slumgullion Landslide Natural Laboratory, *Journal of Geophysical Research: Solid Earth* **116**, B09404, doi:10.1029/2011JB008304.
- 15 Got, J.-L., Mourot, P. and Grangeon, J.: 2010, Pre-failure behaviour of an unstable limestone cliff from displacement and seismic data, *Natural Hazards and Earth System Sciences* **10**(4), 819–829.
- Green, R. G., White, R. S. and Greenfield, T.: 2014, Motion in the north Iceland volcanic rift zone accommodated by bookshelf faulting, *Nature Geoscience* **7**(1), 29–33.
- 20 Greenfield, T. and White, R. S.: 2015, Building Icelandic igneous crust by repeated melt injections, *Journal of Geophysical Research: Solid Earth* **120**(11), 7771–7788.
- Greenfield, Tim, White, Robert S., Ágústsdóttir, Thorbjörg & Winder, Tom. Seismicity of the Askja and Bardarbunga volcanic systems of Iceland, 2009–2015, *Journal of Volcanology and Geothermal Research*, in press.
- Gutenberg, B. and Richter, C.F.: 1956, Magnitude and Energy of Earthquakes, *Annali di Geofisica* **9**, 1–15.
- 25 Gylfadóttir, S. S., Kim, J., Kristinn Helgason, J., Brynjólfsson, S., Höskuldsson, Á., Jóhannesson, T., Bonnevie Harbitz, C. and Løvholt, F.: 2016, The 2014 Lake Askja rockslide tsunami-optimization of landslide parameters comparing numerical simulations with observed run-up, *EGU General Assembly Conference Abstracts*, Vol. 18, p. 8927.
- Gylfadóttir, S. S., Kim, J., Helgason, J. K., Brynjólfsson, S., Höskuldsson, Á., Jóhannesson, T., Harbitz, C. B. and Løvholt, F.: 2017, The 2014 Lake Askja rockslide-induced tsunami: Optimization of numerical tsunami model using observed data,
- 30 *Journal of Geophysical Research: Oceans* **122**, 4110–4122.
- Hammer, C., Beyreuther, M. and Ohrnberger, M.: 2012, A seismic-event spotting system for volcano fast-response systems, *Bulletin of the Seismological Society of America* **102**(3), 948–960.
- Hartley, M. and Thordarson, T.: 2012, Formation of Öskjuvatn caldera at Askja, North Iceland: Mechanism of caldera collapse and implications for the lateral flow hypothesis, *Journal of Volcanology and Geothermal Research* **227**, 85–101.



- Helgason, J. K., Brynjólfsson, S., Jóhannesson, T., S., V. K., Grímsdóttir, H., Hjartardóttir, Á. R., Sæmundsson, Þ., Hóskuldsson, Á., Sigmundsson, F. and Reynolds, H.: 2014, Rockslide in Askja, July 21 2014 - Preliminary results of observations, *Memo of the Icelandic Meteorological Office* pp. 1–12.
- Hellweg, M.: 2000, Physical models for the source of Lascar's harmonic tremor, *Journal of Volcanology and Geothermal Research* **101**(1), 183–198.
- Helmstetter, A. and Garambois, S.: 2010, Seismic monitoring of Séchilienne rockslide (French Alps): Analysis of seismic signals and their correlation with rainfalls, *Journal of Geophysical Research: Earth Surface* **115**, F03016, doi:10.1029/2009JF001532.
- Helmstetter, A., Nicolas, B., Comon, P. and Gay, M.: 2015, Basal icequakes recorded beneath an Alpine glacier (Glacier d'Argentière, Mont Blanc, France): Evidence for stick-slip motion?, *Journal of Geophysical Research: Earth Surface* **120**(3), 379–401.
- Hibert, C., Mangeney, A., Grandjean, G. and Shapiro, N.: 2011, Slope instabilities in Dolomieu crater, Réunion Island: From seismic signals to rockfall characteristics, *Journal of Geophysical Research: Earth Surface* **116**, F04032, doi:10.1029/2011JF002038.
- Hibert, C., Ekström, G. and Stark, C. P.: 2014, Dynamics of the Bingham Canyon Mine landslides from seismic signal analysis, *Geophysical Research Letters* **41**(13), 4535–4541.
- Hibert, C., Mangeney, A., Grandjean, G., Baillard, C., Rivet, D., Shapiro, N.M., Satriano, C., Maggi, A., Boissier, P., Ferrazzini, V. and Crawford, W.: 2014, Automated identification, location, and volume estimation of rockfalls at Piton de la Fournaise volcano, *Journal of Geophysical Research: Earth Surface* **119**(5), 1082–1105.
- Hibert, C., Stark, C. and Ekström, G.: 2015, Dynamics of the Oso-Steelhead landslide from broadband seismic analysis, *Natural Hazards and Earth System Sciences* **15**(6), 1265–1273.
- Hoskuldsson, A., Gans, P., Burbank, D. and Wiss, A.: 2015, Avalanche induced Tsunami in Askja caldera lake Iceland, June 21st. 2014, *EGU General Assembly Conference Abstracts*, Vol. 17, p. 9762.
- Hotovec, A. J., Prejean, S. G., Vidale, J. E. and Gombert, J.: 2013, Strongly gliding harmonic tremor during the 2009 eruption of Redoubt Volcano, *Journal of Volcanology and Geothermal Research* **259**, 89–99.
- Huggel, C., Caplan-Auerbach, J., Gruber, S., Molnia, B. and Wessels, R.: 2008, The 2005 Mt. Steller, Alaska, rock-ice avalanche: A large slope failure in cold permafrost, *Proceedings of the Ninth International Conference on Permafrost*, Vol. 29, pp. 747–752.
- Ito, K. and Enoki, M.: 2007, Acquisition and analysis of continuous acoustic emission waveform for classification of damage sources in ceramic fiber mat, *Materials Transactions* **48**(6), 1221–1226.
- Iverson, R. M., George, D. L., Allstadt, K., Reid, M. E., Collins, B., Vallance, J. W., Schilling, S. P., Godt, J. W., Cannon, C., Magirl, C. S. et al.: 2015, Landslide mobility and hazards: implications of the 2014 Oso disaster, *Earth and Planetary Science Letters* **412**, 197–208.



- Iverson, R. M., Reid, M. E. and LaHusen, R. G.: 1997, Debris-flow mobilization from landslides, *Annual Review of Earth and Planetary Sciences* **25**(1), 85–138.
- Jakobsdóttir, S., Roberts, M., Gudmundsson, G., Geirsson, H. and Slunga, R.: 2008, Earthquake swarms at Uppþyppingar, north-east Iceland: A sign of magma intrusion?, *Studia Geophysica et Geodaetica* **52**(4), 513–528.
- 5 Jakobsdóttir, S. S.: 2008, Seismicity in Iceland: 1994–2007, *Jökull* **58**, 75–100.
- Jakobsdóttir, S. S., Guðmundsson, G. B. and Stefánsson, R.: 2002, Seismicity in Iceland 1991–2000 monitored by the SIL seismic system, *Jökull* **51**, 87–94.
- Jellinek, A. M. and Bercovici, D.: 2011, Seismic tremors and magma wagging during explosive volcanism, *Nature* **470**(7335), 522–525.
- 10 Jousset, P., Neuberg, J. and Sturton, S.: 2003, Modelling the time-dependent frequency content of low-frequency volcanic earthquakes, *Journal of Volcanology and Geothermal Research* **128**(1), 201–223.
- Julian, B. R.: 1994, Volcanic tremor: nonlinear excitation by fluid flow, *Journal of Geophysical Research: Solid Earth* **99**(B6), 11859–11877.
- Kedar, S., Kanamori, H. and Sturtevant, B.: 1998, Bubble collapse as the source of tremor at Old Faithful Geyser, *Journal of Geophysical Research: Solid Earth* **103**(B10), 24283–24299.
- 15 Key, J., White, R., Soosalu, H. and Jakobsdóttir, S.: 2011, Multiple melt injection along a spreading segment at Askja, Iceland, *Geophysical Research Letters* **38**(5), L05301, doi:10.1029/2010GL046264.
- Kolesnikov, Y. I., Nemirovich-Danchenko, M. M., Goldin, S. and Seleznev, V.: 2003, Slope stability monitoring from microseismic field using polarization methodology, *Natural Hazards and Earth System Science* **3**(6), 515–521.
- 20 Konstantinou, K. I. and Schlindwein, V.: 2003, Nature, wavefield properties and source mechanism of volcanic tremor: a review, *Journal of Volcanology and Geothermal Research* **119**(1), 161–187.
- Leet, R. C.: 1988, Saturated and subcooled hydrothermal boiling in groundwater flow channels as a source of harmonic tremor, *Journal of Geophysical Research: Solid Earth* **93**(B5), 4835–4849.
- Lipovsky, B. P. and Dunham, E. M.: 2015, Vibrational modes of hydraulic fractures: Inference of fracture geometry from resonant frequencies and attenuation, *Journal of Geophysical Research: Solid Earth* **120**(2), 1080–1107.
- 25 Lipovsky, B. P. and Dunham, E. M.: 2016, Tremor during ice-stream stick slip, *The Cryosphere* **10**(1), 385–399.
- Lipovsky, B. P. and Dunham, E. M.: 2017, Slow-slip events on the Whillans Ice Plain, Antarctica, described using rate-and-state friction as an ice stream sliding law, *Journal of Geophysical Research: Earth Surface* **122**(4), 973–1003.
- Lockner, D., Byerlee, J., Kuksenko, V., Ponomarev, A. and Sidorin, A.: 1991, Quasi-static fault growth and shear fracture energy in granite, *Nature* **350**(6313), 39–42.
- 30 MacAyeal, D., Okal, E., Aster, R. and Bassis, J.: 2008, Seismic and hydroacoustic tremor generated by colliding icebergs, *Journal of Geophysical Research: Earth Surface* **113**, F03011, doi:10.1029/2008JF001005.
- Manconi, A., Picozzi, M., Coviello, V., De Santis, F. and Elia, L.: 2016, Real-time detection, location, and characterization of rockslides using broadband regional seismic networks, *Geophysical Research Letters* **43**, 6960–6967.



- Marone, C.: 1998, Laboratory-derived friction laws and their application to seismic faulting, *Annual Review of Earth and Planetary Sciences* **26**(1), 643–696.
- Martin, S., Drucker, R., Aster, R., Davey, F., Okal, E., Scambos, T. and MacAyeal, D.: 2010, Kinematic and seismic analysis of giant tabular iceberg breakup at Cape Adare, Antarctica, *Journal of Geophysical Research: Solid Earth* **115**, B06311, doi:10.1029/2009JB006700.
- Matoza, R. S., Fee, D. and Garcés, M. A.: 2010, Infrasonic tremor wavefield of the PuuŌō crater complex and lava tube system, Hawaii, in April 2007, *Journal of Geophysical Research: Solid Earth* **115**, B12312, doi:10.1029/2009JB007192.
- McLaskey, G. C. and Glaser, S. D.: 2011, Micromechanics of asperity rupture during laboratory stick slip experiments, *Geophysical Research Letters* **38**, L12302, doi:10.1029/2011GL047507.
- McNutt, S. R.: 1992, Volcanic tremor, *Encyclopedia of earth system science* **4**, 417–425.
- McNutt, S. R.: 2005, Volcanic seismology, *Annual Review of Earth and Planetary Sciences* **32**, 461–491.
- Mitchell, M. A., White, R. S., Roecker, S. and Greenfield, T.: 2013, Tomographic image of melt storage beneath Askja Volcano, Iceland using local microseismicity, *Geophysical Research Letters* **40**(19), 5040–5046.
- Moore, J. G.: 2001, Density of basalt core from Hilo drill hole, Hawaii, *Journal of Volcanology and Geothermal Research* **112**(1), 221–230.
- Moretti, L., Mangeny, A., Capdeville, Y., Stutzmann, E., Huggel, C., Schneider, D. and Bouchut, F.: 2012, Numerical modeling of the Mount Steller landslide flow history and of the generated long period seismic waves, *Geophysical Research Letters* **39**, L16402, doi:10.1029/2012GL052511.
- Moretti, L., Allstadt, K., Mangeny, A., Capdeville, Y., Stutzmann, E. and Bouchut, F.: 2015, Numerical modeling of the Mount Meager landslide constrained by its force history derived from seismic data, *Journal of Geophysical Research: Solid Earth* **120**(4), 2579–2599.
- Nadeau, R. M. and Johnson, L. R.: 1998, Seismological studies at Parkfield VI: Moment release rates and estimates of source parameters for small repeating earthquakes, *Bulletin of the Seismological Society of America* **88**(3), 790–814.
- Neuberg, J.: 2000, Characteristics and causes of shallow seismicity in andesite volcanoes, *Philosophical Transactions of the Royal Society of London A: Mathematical, Physical and Engineering Sciences* **358**(1770), 1533–1546.
- Neuberg, J. and O’Gorman, C.: 2002, A model of the seismic wavefield in gas-charged magma: application to Soufriere Hills Volcano, Montserrat, *Geological Society, London, Memoirs* **21**(1), 603–609.
- Norris, R. D.: 1994, Seismicity of rockfalls and avalanches at three Cascade Range volcanoes: Implications for seismic detection of hazardous mass movements, *Bulletin of the Seismological Society of America* **84**(6), 1925–1939.
- Okal, E. A.: 1990, Single forces and double-couples: a theoretical review of their relative efficiency for the excitation of seismic and tsunami waves, *Journal of Physics of the Earth* **38**(6), 445–474.
- Omori, F.: 1894, On the Aftershocks of Earthquakes, *Journal of the College of Science, Imperial University of Tokyo* **7**, 111–120.
- Palmer, J.: 2017, creeping earth could hold secret to deadly landslides, *Nature* **548**(7668), 384–386.



- Powell, T. and Neuberg, J.: 2003, Time dependent features in tremor spectra, *Journal of Volcanology and Geothermal Research* **128**(1), 177–185.
- Rice, J. R., Lapusta, N. and Ranjith, K.: 2001, Rate and state dependent friction and the stability of sliding between elastically deformable solids, *Journal of the Mechanics and Physics of Solids* **49**(9), 1865–1898.
- 5 Rööfli, C., Walter, F., Husen, S., Andrews, L. C., Lüthi, M. P., Catania, G. A. and Kissling, E.: 2014, Sustained seismic tremors and icequakes detected in the ablation zone of the Greenland ice sheet, *Journal of Glaciology* **60**(221), 563–575.
- Rust, A., Balmforth, N. and Mandre, S.: 2008, The feasibility of generating low-frequency volcano seismicity by flow through a deformable channel, *Geological Society, London, Special Publications* **307**(1), 45–56.
- Saemundsson, T., Kristinn Helgason, J., Brynjólfsson, S., Hoskuldsson, A., Rut Hjartardóttir, A. and Sigmundsson, F.: 2015, 10 The rockslide in the Askja caldera on the 21st of July 2014, *EGU General Assembly Conference Abstracts*, Vol. 17, p. 11734.
- Sassa, K., Dang, K., Yanagisawa, H. and He, B.: 2016, A new landslide-induced tsunami simulation model and its application to the 1792 Unzen-Mayuyama landslide-and-tsunami disaster, *Landslides* **13**(6), 1405–1419.
- Schlindwein, V., Wassermann, J. and Scherbaum, F.: 1995, Spectral analysis of harmonic tremor signals at Mt. Semeru 15 volcano, Indonesia, *Geophysical Research Letters* **22**(13), 1685–1688.
- Schneider, D., Bartelt, P., Caplan-Auerbach, J., Christen, M., Huggel, C. and McArdell, B. W.: 2010, Insights into rock-ice avalanche dynamics by combined analysis of seismic recordings and a numerical avalanche model, *Journal of Geophysical Research: Earth Surface* **115**, F04026, doi:10.1029/2010JF001734.
- Senfaute, G., Duperret, A. and Lawrence, J.: 2009, Micro-seismic precursory cracks prior to rock-fall on coastal chalk cliffs: 20 a case study at Mesnil-Val, Normandie, NW France, *Natural Hazards and Earth System Sciences* **9**(5), 1625–1641.
- Shelly, D. R., Beroza, G. C., Ide, S. and Nakamura, S.: 2006, Low-frequency earthquakes in Shikoku, Japan, and their relationship to episodic tremor and slip, *Nature* **442**(7099), 188.
- Shelly, D. R., Beroza, G. C. and Ide, S.: 2007, Non-volcanic tremor and low-frequency earthquake swarms, *Nature* **446**(7133), 305.
- 25 Sigvaldason, G. E.: 2002, Volcanic and tectonic processes coinciding with glaciation and crustal rebound: an early Holocene rhyolitic eruption in the Dyngjufjöll volcanic centre and the formation of the Askja caldera, north Iceland, *Bulletin of Volcanology* **64**(3–4), 192–205.
- Sima, H.: 1986, On Observation of Microearthquakes as Events Preceding the Jizukiyama Landslide, Nagano Prefecture, *Journal of Japan Landslide Society* **23**(1), 1–7.
- 30 Soosalu, H., Key, J., White, R. S., Knox, C., Einarsson, P. and Jakobsdóttir, S. S.: 2010, Lower-crustal earthquakes caused by magma movement beneath Askja volcano on the north Iceland rift, *Bulletin of Volcanology* **72**(1), 55–62.
- Sturton, S. and Neuberg, J.: 2006, The effects of conduit length and acoustic velocity on conduit resonance: Implications for low-frequency events, *Journal of Volcanology and Geothermal Research* **151**(4), 319–339.



- Suriñach, E., Vilajosana, I., Khazaradze, G., Biescas, B., Furdada, G. and Vilaplana, J.: 2005, Seismic detection and characterization of landslides and other mass movements, *Natural Hazards and Earth System Science* **5**(6), 791–798.
- Takei, Y. and Kumazawa, M.: 1994, Why have the single force and torque been excluded from seismic source models?, *Geophysical Journal International* **118**(1), 20–30.
- 5 Thorarinsson, S. and Sigvaldason, G. E.: 1962, The eruption in Askja, 1961; a preliminary report, *American Journal of Science* **260**(9), 641–651.
- Tonnellier, A., Helmstetter, A., Malet, J.-P., Schmittbuhl, J., Corsini, A. and Joswig, M.: 2013, Seismic monitoring of soft-rock landslides: the Super-Sauze and Valoria case studies, *Geophysical Journal International* **193**(3), 1515–1536.
- Unglert, K. and Jellinek, A.: 2015, Volcanic tremor and frequency gliding during dike intrusions at Kīlauea – A tale of three  
10 eruptions, *Journal of Geophysical Research: Solid Earth* **120**(2), 1142–1158.
- Van Genuchten, P. and De Rijke, H.: 1989, On pore water pressure variations causing slide velocities and accelerations observed in a seasonally active landslide, *Earth Surface Processes and Landforms* **14**(6), 577–586.
- Vilajosana, I., Suriñach, E., Abellán, A., Khazaradze, G., Garcia, D. and Llosa, J.: 2008, Rockfall induced seismic signals: case study in Montserrat, Catalonia, *Natural Hazards and Earth System Science* **8**(4), 805–812.
- 15 Vogfjörð, K., Kristinn Helgason, J., Jonsdóttir, K., Brynjólfsson, S., Grimsdóttir, H., Johannesson, T., Hensch, M. and Ripepe, M.: 2015, The Askja rockslide and the associated tsunami in the caldera lake, *EGU General Assembly Conference Abstracts*, Vol. 17, p. 12128.
- Voight, B., Glicken, H., Janda, R. and Douglass, P.: 1981, Catastrophic rockslide avalanche of May 18, in P. Lipman and D. Mullineaux (eds), *The 1980 Eruptions of Mount St. Helens, Washington*, Vol. 1250, US Geological Survey Professional  
20 Papers, pp. 347–377.
- Vouillamoz, N., Rothmund, S., Joswig, M., Malet, J.-P. and Jochum, B.: 2017, Passive seismic monitoring of landslides' creep: Case studies at Super-Sauze (Southeastern France) and Pechgraben (Upper Austria) clay-rich landslides, *EGU General Assembly Conference Abstracts*, Vol. 19, p. 9561.
- Walter, F., Roux, P., Roeoesli, C., Lecointre, A., Kilb, D. and Roux, P.-F.: 2015, Using glacier seismicity for phase velocity  
25 measurements and Green's function retrieval, *Geophysical Journal International* **201**(3), 1722–1737.
- Walter, M., Amhardt, C. and Joswig, M.: 2012, Seismic monitoring of rockfalls, slide quakes, and fissure development at the Super-Sauze mudslide, French Alps, *Engineering Geology* **128**, 12–22.
- Wessel, P., Smith, W. H., Scharroo, R., Luis, J. and Wobbe, F.: 2013, Generic mapping tools: improved version released, *Eos, Transactions American Geophysical Union* **94**(45), 409–410.
- 30 White, R. S., Drew, J., Martens, H. R., Key, J., Soosalu, H. and Jakobsdóttir, S. S.: 2011, Dynamics of dyke intrusion in the mid-crust of Iceland, *Earth and Planetary Science Letters* **304**(3), 300–312.
- Wiens, D. A., Anandkrishnan, S., Winberry, J. P. and King, M. A.: 2008, Simultaneous teleseismic and geodetic observations of the stick-slip motion of an Antarctic ice stream, *Nature* **453**(7196), 770–775.





- Winberry, P. J., Anandakrishnan, S., Wiens, D. A. and Alley, R. B.: 2013, Nucleation and seismic tremor associated with the glacial earthquakes of Whillans Ice Stream, Antarctica, *Geophysical Research Letters* **40**(2), 312–315.
- Yamada, M., Kumagai, H., Matsushi, Y. and Matsuzawa, T.: 2013, Dynamic landslide processes revealed by broadband seismic records, *Geophysical Research Letters* **40**(12), 2998–3002.
- 5 Yamada, M., Mori, J. and Matsushi, Y.: 2016, Possible stick-slip behavior before the Rausu landslide inferred from repeating seismic events, *Geophysical Research Letters* **43**(17), 9038–9044.
- Zeckra, M., Hovius, N., Burtin, A. and Hammer, C.: 2015, Automated Detection and Classification of Rockfall Induced Seismic Signals with Hidden-Markov-Models, *AGU Fall Meeting 2015*, abstract #NH34A-04.
- Zigone, D., Voisin, C., Larose, E., Renard, F. and Campillo, M.: 2011, Slip acceleration generates seismic tremor like signals  
10 in friction experiments, *Geophysical Research Letters* **38**, L01315, doi:10.1029/2010GL045603.

**Table 1****Parameters of the stick-slip simulations**

Parameter	Symbol	Value
Epicentral distance	L	3.5 km
Quality factor	Q	25
Shear wave speed in rock	$c_s$	1878 m s <sup>-1</sup>
Density of rock	$\rho$	2000 kg m <sup>-3</sup>
Thickness of landslide	H	30 m
Frictional state evolution distance	$d_c$	15x10 <sup>-6</sup> m
Frictional direct effect parameter	a	0.03
Frictional ageing effect parameter	b	0.04
Static coefficient of friction	$\mu_0$	0.7
Initial loading velocity	$v_0$	0.6 mm s <sup>-1</sup>
Repeating earthquake patch radius	R	40 m
Creep acceleration on the accelerating patch	$\dot{v}_1$	+0.01 (mm s <sup>-1</sup> )min <sup>-1</sup>
Creep deceleration on the decelerating patch	$\dot{v}_2$	-0.01 (mm s <sup>-1</sup> )min <sup>-1</sup>

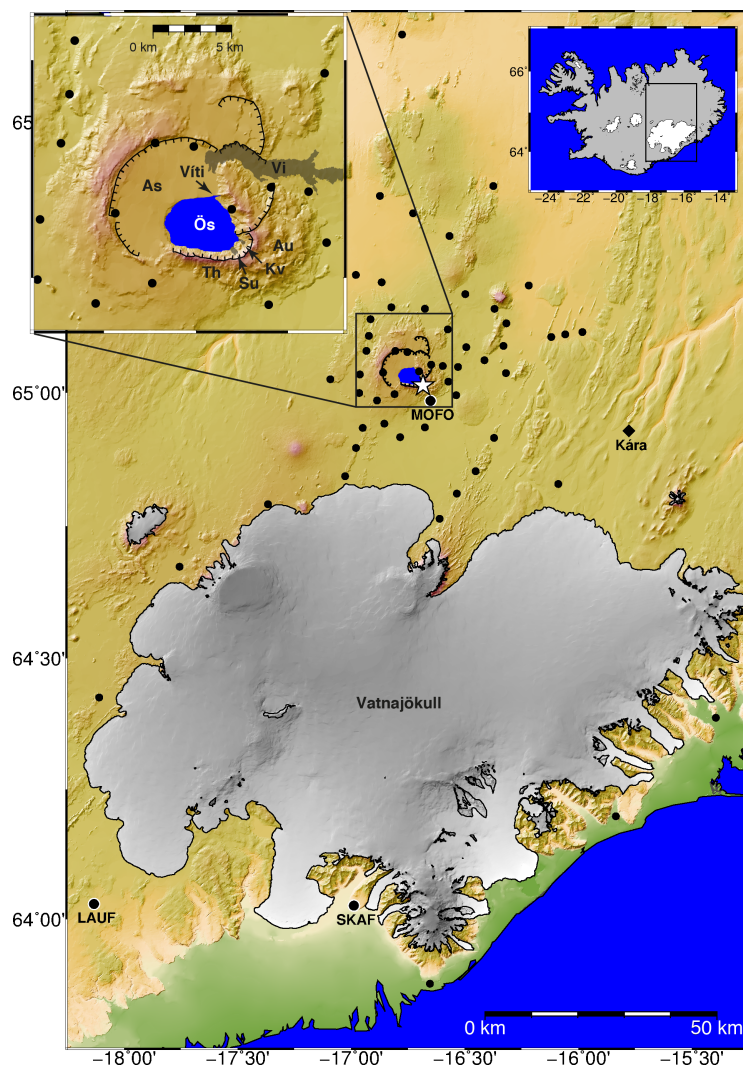


Figure 1: The Askja central volcano north of the ice cap Vatnajökull in the Icelandic highlands with locations of the seismic stations (black circles). The white star is the source location of the 21 July 2014 landslide. The weather station Kárahnjúkar is indicated with a black diamond. Inset of the Askja central volcano shows the hyaloclastite mountains of Austurfjöll (Au) and Thorvaldsfjall (Th), the caldera ring faults of the Askja caldera (As) and the Öskjuvatn caldera (Ös), the small explosion crater Viti, the basaltic 1922/23 eruption sites of Suðurbotnahraun (Su) and Kvislahraun (Kv), and the 1961 Vikrahraun (Vi) lava flow.

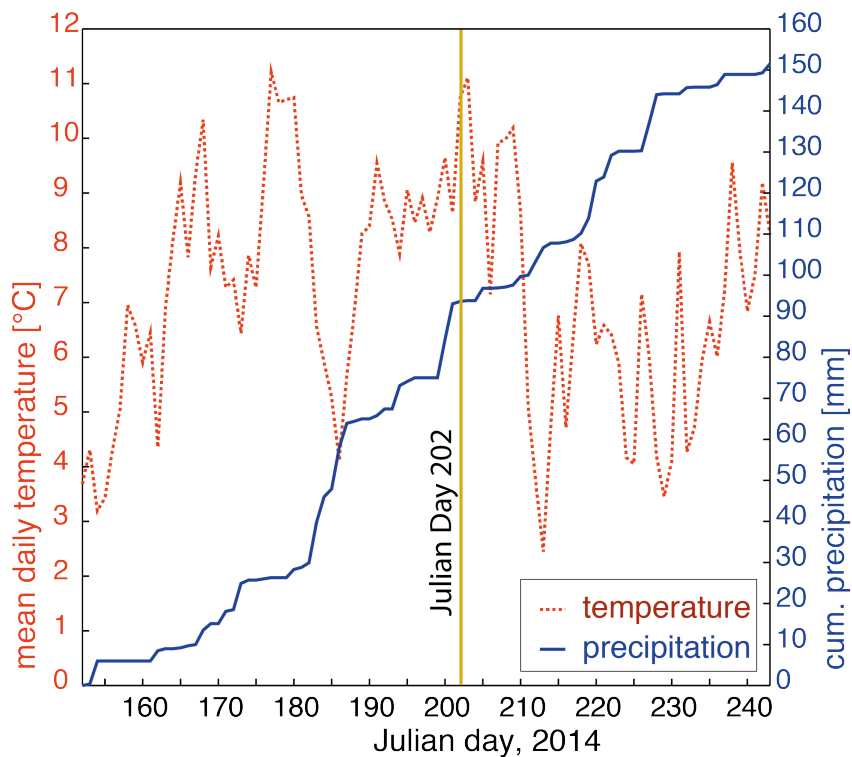
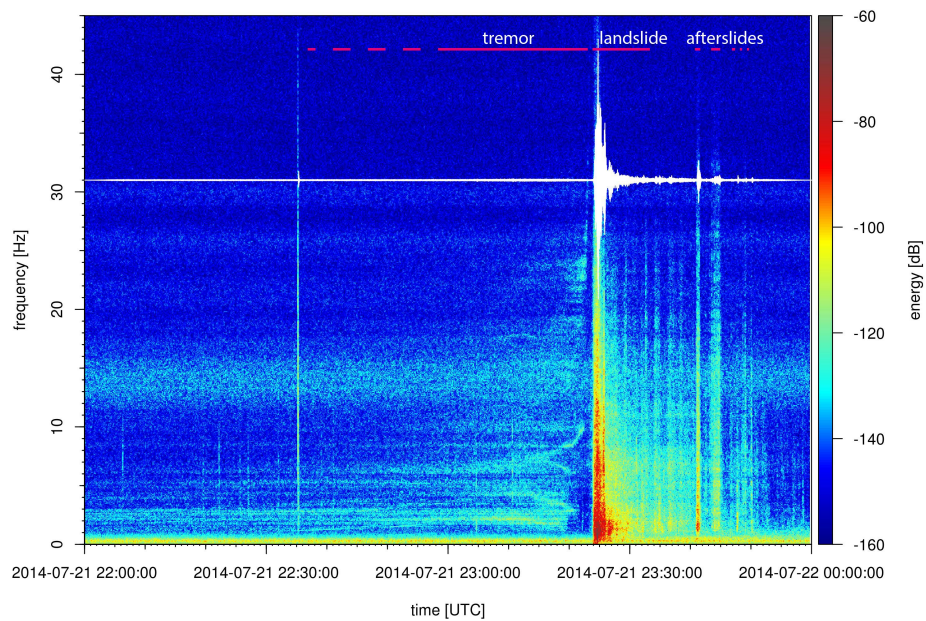


Figure 2: Mean daily temperatures and cumulative precipitation at weather station Kárahnjúkar (see Fig. 1 for location) in June, July and August 2014. Note the two days with high precipitation immediately before and the increased temperature at the day of the landslide (Julian Day 202, yellow line).

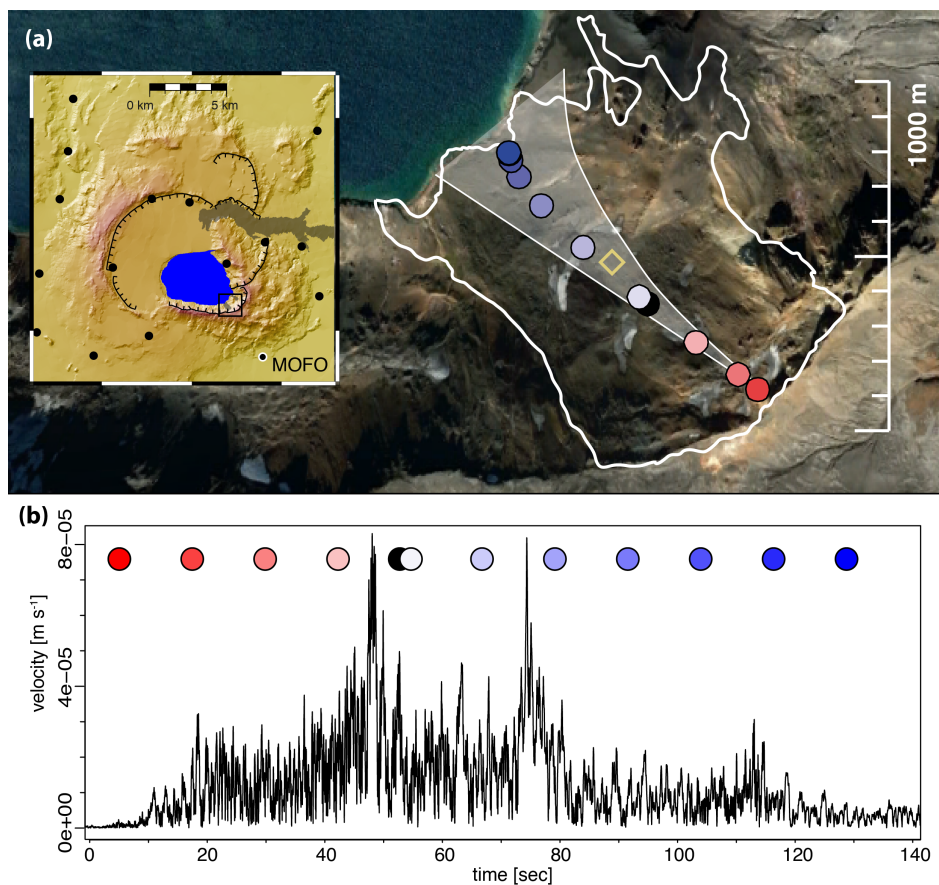
5



**Figure 3: Cracks on top of the landslide body in August 2013, a year before the failure. Location of the image is indicated on Fig. 5, view is to the west. Image taken by Daniele Trippanera.**



**Figure 4:** Spectrogram of the landslide and its precursory tremor at the Askja caldera on 21 July 2014. White trace is the waveform of the signal filtered between 1–45 Hz. Station MOFO, vertical component.



5 **Figure 5:** (a) Path of the landslide bulk volume from the landslide force history inversion of the seismic waveforms between 0.02-0.08Hz. Red circles mark the acceleration phase, the black circle is the transition to the deceleration phase (blue circles). Shaded white area is the range of the inversion results with different frequencies of the band pass filter (0.02-0.05 Hz, 0.02-0.08 Hz, 0.04-0.08 Hz). The white line is the outline of the landslide source area. The yellow diamond is the location of Fig. 3. The black square on the inset shows the location of the main image. (b) Envelope of the East component of station MOFO (see inset for location), filtered between 1-45Hz and the time evolution of the landslide acceleration (red circles) and deceleration (blue circles). Start of the x axis is at 23:24:05 UTC.

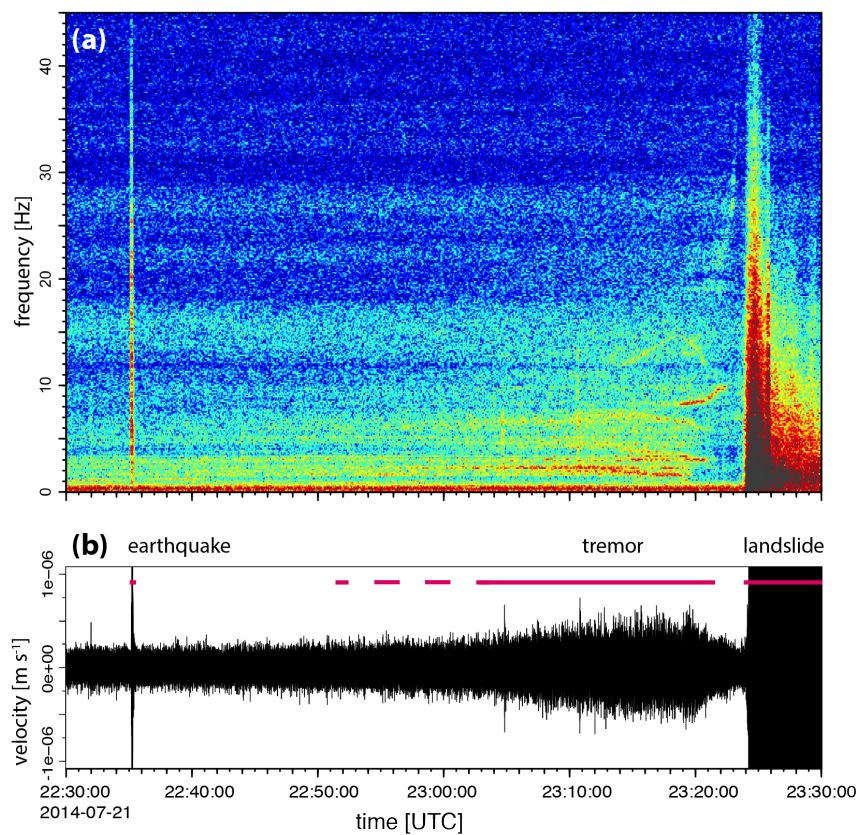


Figure 6: (a) Spectrogram and (b) waveform (filtered between 1–45Hz) of the tremor signal preceding the 21 July 2014 landslide. Station MOFO, East component. Colour scale for the spectrogram is the same as in Fig. 4.

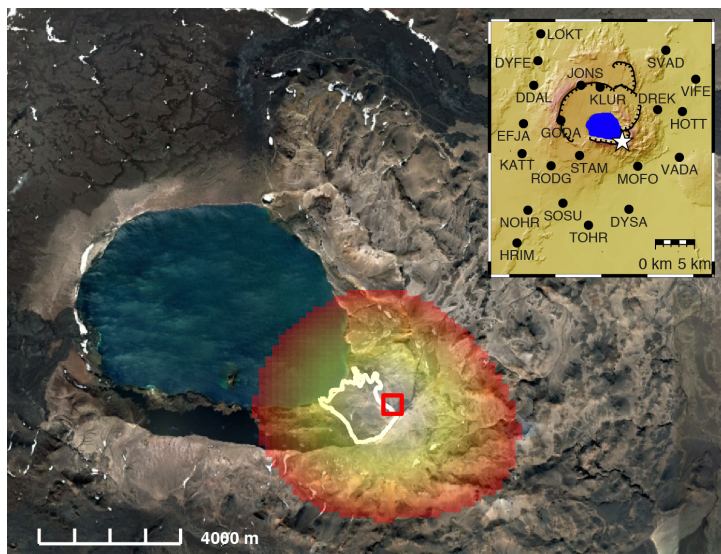
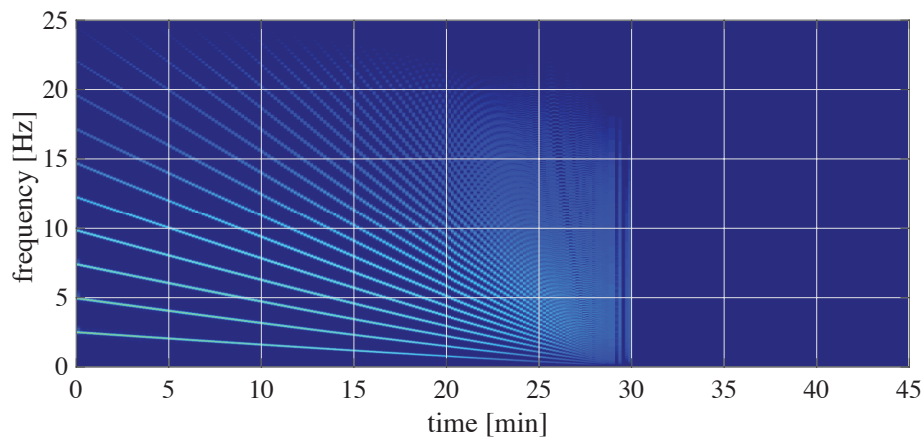


Figure 7: Example of the localisation results of the tremor using the tremor record between 23:00:00 and 23:01:00 UTC, filtered between 1.5–3 Hz and a seismic wave velocity of 2300m/s. The open red square is the best fit location and the ellipse around it is the likelihood quantile from 0.997 (red) to 1 (translucent white). The white line is the outline of the landslide source area. The inset shows the locations of the seismic stations used in the localisation and the location of the landslide source area (white star).

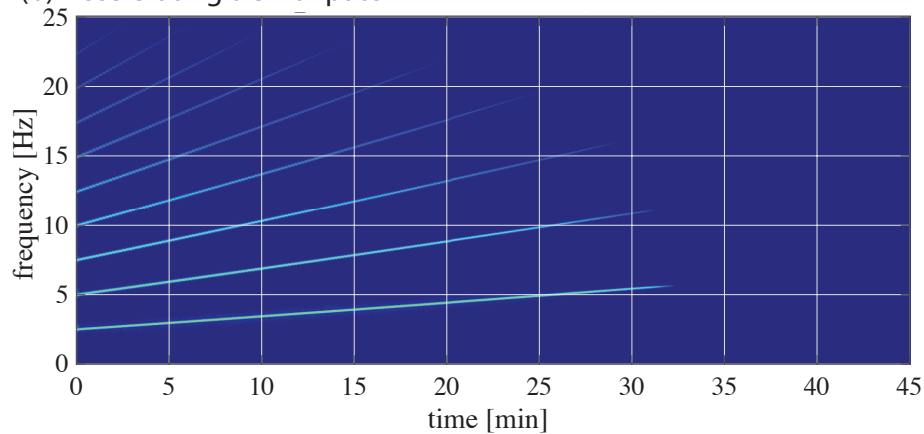




(a) Decelerating tremor patch



(b) Accelerating tremor patch



5 **Figure 8:** Result of the stick-slip simulations with a patch size of radius 40 m and a landslide thickness of 30 m. The spectrogram is calculated for a receiver station 3.5 km away from the location of the stick-slip events (comparable to the distance of station MOFO to the landslide source area) and the colour scale is the same as in Fig. 4. (a) shows the simulation result for a decelerating tremor patch where the time between stick-slip earthquakes increases. (b) shows the simulation result for an accelerating tremor patch where the time between stick-slip earthquakes decreases.

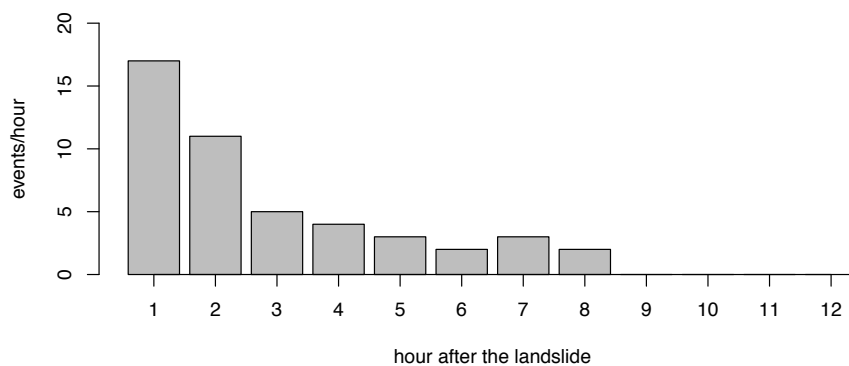


Figure 9: Numbers of small slope failures after the Askja landslide per hour.